Violin bow vibrations

Colin E. Gough[a)]
School of Physics and Astronomy, University of Birmingham, Birmingham B15 2TT, United Kingdom

(Received 27 October 2011; revised 21 February 2012; accepted 23 February 2012)

The modal frequencies and bending mode shapes of a freely supported tapered violin bow are investigated by finite element analysis and direct measurement, with and without tensioned bow hair. Such computations are used with analytic models to model the admittance presented to the stretched bow hairs at the ends of the bow and to the string at the point of contact with the bow. Finite element computations are also used to demonstrate the influence of the lowest stick mode vibrations on the low frequency bouncing modes, when the hand-held bow is pressed against the string. The possible influence of the dynamic stick modes on the sound of the bowed instrument is briefly discussed. © *2012 Acoustical Society of America*. [http://dx.doi.org/10.1121/1.3699172]

PACS number(s): 43.75.De, 43.40.At, 43.40.Cw [JW] Pages: 4152–4163

I. INTRODUCTION

In contrast to the large number of research papers on the vibrational modes of the violin, relatively few have been published on the bow. This is somewhat surprising, as the bow is a much simpler structure to understand and is believed by most violinists to have a major influence on the sound of any bowed instrument. However, the exact way in which the vibrational modes of the bow influence the sound of the violin remains an open question.

The first significant modern research on the vibrational modes of the bow in 1975 was a pioneering theoretical and experimental investigation by Schumacher[1] on a freely supported bow. This was followed in the 1990s by a series of important papers by Askenfelt[2–4] and Bissinger[5,6] reporting modal frequencies and mode shapes of the freely supported bow in addition to identifying the *bouncing* modes of the bow, when resting on the string and pivoted about the frog.

Askenfelt and Guettler[7–9] have more recently demonstrated the important influence of the bouncing modes on both short bowed strokes (e.g., sautillé, spiccato, ricochet, martelé, etc.) and the initial transients of any strongly attacked longer bow stroke. Guettler has also contributed an important chapter on the bow and bowed string in *The Science of String Instruments*.[10]

Because the diameter of the bow stick is small compared with the wavelength of the radiated sound, significant direct radiation from the bow is unlikely. This is easily demonstrated by striking the tensioned bow hair against the edge of any heavy body. Almost no sound is heard after the initial impact, even though the bow stick is seen and felt to continue vibrating very strongly.

As Schumacher[1] recognized, it is more likely that the stick vibrations could influence the radiated sound via their coupling to the transverse and longitudinal waves of the bow hair. Such vibrations, excited on impact with the string, will result in periodic fluctuations of both the force and the relative velocity between bow hair and string at the point of contact.

Both effects could, in principle, affect the excitation of Helmholtz kinks via the slip-stick mechanism[11] and hence the spectrum of the radiated sound, as described by Cremer[12] (Chap. 5).

In a previous paper,[13] analytic, computational, and direct measurements were used to examine the influence of taper and camber on the low frequency dynamics and elastic properties of the bow. In this paper, a similar approach is used to examine the vibrational modes of the bow and their potential influence on the sound of the instrument via their coupling to the vibrating string and hence to the radiating modes of the violin body.

II. STICK MODES

A. Introduction

Figure 1 defines the orthogonal set of axis and geometry used to describe the vibrational modes of the bow and coupled bow hair. It illustrates the way that the vibrations of the head of the bow can couple to the various modes of vibration of the bow hair, which via the hair-string contact could either transfer energy to the radiating modes of the violin body or influence the generation of circulating Helmholtz kinks on the string.

For a continuously bowed note, the slip-stick generation of Helmholtz kinks will depend on the downward force of the bow on the string, which will be influenced by transverse vibrations of the bow in the *y*-direction. The relative velocity of string and hair at the point of bow contact will be influenced by the longitudinal vibrations of the bow hair excited by the in-plane (*xy*-plane) rotations and longitudinal (*y*-direction) vibrations of the bow head. The circulating kinks on the bow hair excited by the slip-stick mechanism will, in turn, excite both *in-* and *out-of-plane* vibrations of the bow stick under normal playing conditions, when the bow stick is tipped on its longitudinal axis away from the bridge.

B. The freely supported bow

First consider the vibrations of a highly simplified bow model[13] comprising a constant diameter straight bow stick with equal length rigid levers at its ends representing the frog

a)Author to whom correspondence should be addressed. Electronic mail: profgough@googlemail.com

 0001-4966/2012/131(5)/4152/12/$30.00

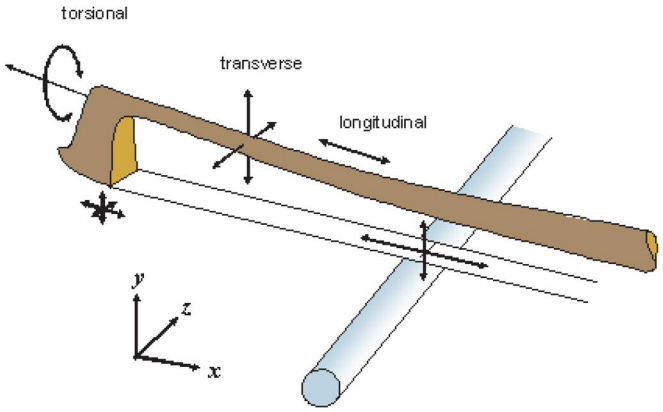

FIG. 1. (Color online) The geometry of the bow and string illustrating the polarization directions of the two bending, the longitudinal and torsional modes of the bow stick, and their coupling to the stretched bow hairs.

and head of the bow, between which the bow hair would normally be stretched.

The important bending modes will have frequencies and mode shapes closely related to the bending modes of a uniform cross-section slender bar weakly perturbed by the additional masses of the frog and head at the ends of the bow stick.

For a slender, uniform properties, constant cross-section bar of radius a and length l, the bending wave displacements satisfy the wave equation

$$EK^2 \frac{d^4y}{dx^4} = \rho \frac{d^2y}{dt^2}, \tag{1}$$

where E is the elastic constant, $K = a/2$ the *radius of gyration* of the bar, and ρ its density.

For a freely suspended bar, the vibrational frequencies are given by

$$f_n = \frac{\pi a}{16\ell^2}\sqrt{\frac{E}{\rho}}[3.01^2, 5^2, 7^2, ..., (2n+1)^2] \tag{2}$$

where n is an integer defining the mode number (see, for example, Fletcher and Rossing[14]).

For a freely supported bar, the boundary conditions of zero external couple and force requires the second and third spatial derivatives of the displacements at each end to be zero. This results in a combination of wave-like and exponentially decaying solutions for the displacements y varying with distance $|x|$ from each end approximately as $[\sin(k_n|x| - \pi/4) - e^{-k_n|x|}/\sqrt{2}]e^{i\omega_n t}$, with $\omega_n = \sqrt{EK^2/\rho}k_n^2$. Apart from a small correction from the decaying exponential component of the wave solution from the far end of the bar, the outermost nodes of the sinusoidal spatial components are located at almost exactly $\lambda_n/8$ from the ends of the bar, so that $l \approx (n+1/2)\lambda/2$ with mode frequencies given by Eq. (2). Adding the frog and head of the bow inhibits motion at the ends of the stick, with the outermost nodes moving closer to the ends of the bar. This decreases the mode frequencies with the $(2n+1)^2$ terms approaching $(2n)^2$ for heavy additional end masses. For example, Bissinger and Ye[6] observed

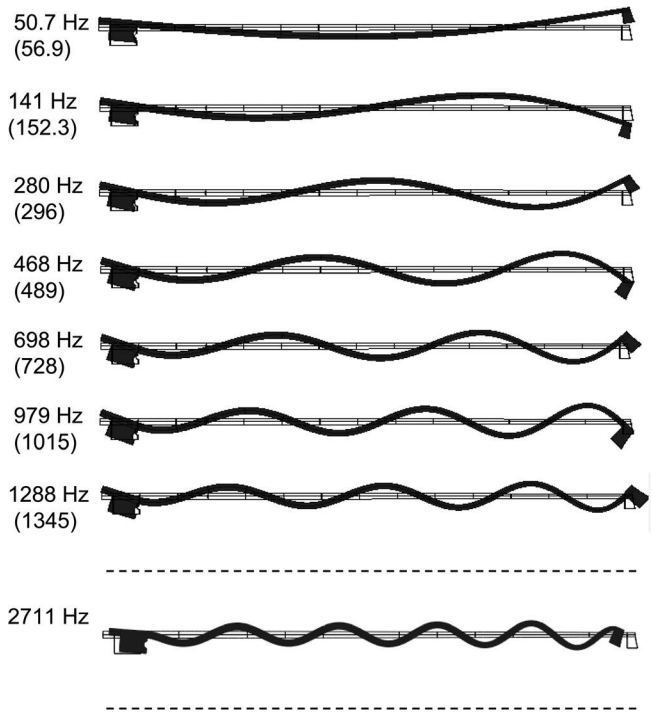

FIG. 2. The first seven in-plane bending modes and frequencies of a straight, Tourte-tapered, violin stick with attached frog and one higher mode illustrating bending-longitudinal wave coupling. The frequencies in brackets are those with the frog removed. An additional example of a higher mode is illustrated showing coupling to longitudinal vibrations of the tapered stick.

a 2.6% drop in stick frequencies on holding the bow at the frog relative to being freely suspended, accompanied by a fractional increase in damping of almost 2.5.

Figure 2 illustrates the first seven in-plane bending modes and a higher mode illustrating coupling to the longitudinal vibrations of the stick. The modes are for a freely supported straight but tapered violin bow, with attached head and frog but no bow hair. The computations used COMSOL finite element software.[15] The finite element geometric model is described in an earlier paper.[13] The stick is 70 cm long with a Tourte-Vuillaume tapered diameter[16] increasing from 5.3 mm at the tip-end to 8.6 mm over the upper 59 cm of the stick. The assumed taper varies with diameter as

$$d(x) = -6.22 + 5.14\log(x + 175), \tag{3}$$

where x is measured from the upper end of the tapered stick with all distances in mm. The diameter of the lower 110 mm of the stick on which the stick is held and the frog slides is constant at 8.6 mm. The computations assume a uniform along-grain elastic constant of 22 GPa and a density of 1200 kgm^{-3} (typical values cited by Askenfelt[4]). The shaped head of the bow and frog were assumed to be rigid with masses of 1.2 g and 10 g, respectively. The resulting mass M of the bow (without hair, screw, end-button and leather/metal-wire protective bindings) was ~49 g. The illustrated modes and frequencies are for the stick with bow head and frog attached. The figures in brackets list the increased modal frequencies on removal of the frog.

Note the increased amplitude and decreased wavelength of the bending modes in the upper half of the bow resulting

from the reduced diameter and consequent increased flexibility. More important are the hatchet-like rotations of both the head of the bow and, to a lesser extent, the frog resulting from the bending deflections at the "free" ends of the bow.

This results in both vertical and horizontal vibrations at both ends of the stretched bow hair. Such motion leads to strong coupling to the transverse and longitudinal vibrations of the bow hair, both of which could, in principle, affect the slip-stick excitation of Helmholtz kinks, as described by Schumacher.[1]

To conserve linear momentum along the length of the freely supported bow, the rotations of the head of the bow induce a coupling to the longitudinal vibrations of the bow stick. This results in the coupled $\lambda_L/2$-longitudinal and bending wave mode at 2.71 kHz illustrated in Fig. 2.

Table I compares the modal frequencies of a freely supported, constant diameter, slender beam with those computed using the finite element model for the Tourte-tapered bow. Additional comparisons are made with the measurements by Askenfelt[4] on a bow of unspecified origin and some measurements of our own on a number of bows of varying quality. The modal frequencies are for the *xy,* in-plane, vibrations of the bow.

The bending mode frequencies of the ideal uniform beam have been uniformly scaled so that the frequency of the 2nd mode is identical to the computed value for the tapered bow. The figures in italics in Table I show the ratio of mode frequencies to that of the 2nd mode, allowing easy comparisons between the theoretical, computed and measured values unaffected by global scaling factors like density, elastic constant, and length and diameter. The normalization has been made to the second mode rather than the fundamental, as the higher order modes are less strongly perturbed by coupling to the vibrations of the tensioned hair.

TABLE I. The frequencies (Hz) of the first seven in-plane modes of a freely supported slender beam compared with finite element predictions for a Tourte-tapered bow stick with a 1.2 g head without frog and measured modal frequencies for a number of untensioned bows of varying quality. The numbers in italics indicate the ratio of mode frequencies to that of the 2nd mode.

Mode number	1	2	3	4	5	6	7
Simple beam	54.8	152.3	299	493	737	1030	1371
	0.360	*1*	*1.96*	*3.24*	*4.84*	*6.76*	*9.00*
Computed without frog	56.9	152.3	296	489	728	1015	1345
	0.374	*1*	*1.95*	*3.21*	*4.78*	*6.66*	*8.83*
Computed with frog	50.7	141	280	468	698	979	1288
	0.360	*1*	*1.99*	*3.32*	*4.95*	*6.94*	*9.13*
Askenfelt (unspecified)	60	160	300	500	750	1000	1300
	0.381	*1*	*1.88*	*3.13*	*4.69*	*6.25*	*8.13*
Bausch	62	159	306	537	785	983	1291
	0.390	*1*	*1.92*	*3.38*	*4.94*	*6.18*	*8.12*
Hill	55	148.1	328	479	743	920	1183
	0.371	*1*	*2.21*	*3.23*	*5.01*	*6.21*	*7.99*
Sartori	59	147.3	326.4	464.1	735.2	927	1139
	0.40	*1*	*2.22*	*3.16*	*4.99*	*6.29*	*7.73*
Antoni	50	138	267	422	590	860	1049
	0.360	*1*	*1.94*	*3.05*	*4.27*	*6.23*	*7.60*

The ratios and absolute values of the modal frequencies of a simple beam are very similar to those computed and measured for real bows, as previously noted by Askenfelt,[2] despite the inevitable differences in their tapers, cambers and additional frog and bow head masses. Nevertheless, there are significant (~10%) variations in the ratios of the modal frequencies. Such variations reflect differences in taper and variations in elastic constant and density along the length of real bows and, to a lesser extent, variations in their bending profiles. However, apart from the lower modal frequencies of the Antoni bow provided with an inexpensive electric violin, there are no dramatic differences between the modal frequencies or their ratios that could be used to correlate reliably with bow quality. The measurements were all made with a fairly relaxed bow tension, to avoid significant perturbation from coupling to any attached bow hair.

In addition to the in-plane bending modes, there is an equivalent set of out-of-plane bending modes, shown in Fig. 3. The mode shapes illustrate the net amplitude of bow displacements on the surface of the bow. This includes circumferential displacements from induced torsional vibrations in addition to the transverse bending deflections. The torsional vibrations are excited by the need to conserve the axial angular momentum of the bow resulting from the sideways swinging of the head and to a lesser extent the frog. This accounts for the apparent thickening of the mode shapes, when significant torsional vibrations are excited.

Further evidence for the coupling of the in- and out-of-plane bending waves to the longitudinal and torsional

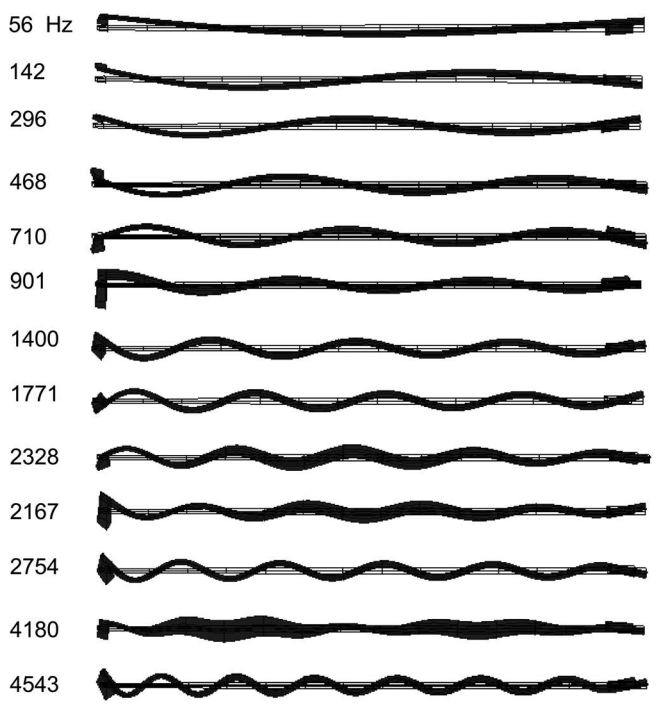

FIG. 3. Out-of-plane bending modes of a straight, Tourte-tapered, bow for a number of illustrative modes. The plots illustrate the total displacements of the stick, bow head, and frog with no bow hair attached including the coupled torsional vibrations resulting in a thickening of the mode shapes.

vibrations of the bow stick will be demonstrated in the next subsection on the admittance at the edge of the bow head supporting the bow hair.

C. Bow stick effective masses and admittances

The dynamical properties of the bow stick can be characterized by the admittance of the bow at the supported ends of the stretched bow hair. For completeness, this would require admittances to be measured in all three orthogonal directions at both ends of the bow. However, because the vibrational amplitudes at the head end of the bow are always considerably larger than those at the frog, as a first approximation, the problem can be simplified by focusing on the admittances and subsequent coupling to the tensioned bow hair at the bow head alone.

The complex admittance of the nth stick mode measured in the x-direction at the central point of hair support on the head of the bow can be written as

$$A_{n,x}(\omega) = \frac{v_{n,x}(\omega)}{F_x} = \frac{i\omega}{m_{n,x}} \frac{1}{\omega_n^2 - \omega^2 + i\omega\omega_n/Q_n}, \tag{4}$$

where $v_{n,x}$ is the velocity of the nth mode induced by an applied sinusoidal force of amplitude F_x in the same direction, ω_n is the resonant angular frequency of the selected mode, Q_n its Q-value, and $m_{n,x}$ its effective mass in the x-direction at the point of measurement. The in-line effective mass is defined by attributing all the kinetic energy KE_n of an excited mode to an effective point mass $m_{n,x}$ at the point of excitation, such that

$$\frac{1}{2} m_{n,x} v_{n,x}^2 = KE_n. \tag{5}$$

Equivalent expressions can be used to describe the effective masses and admittances in the y- and z-directions.

Table II lists the computed effective masses of the modeled Tourte-Vuillaume tapered bow, at the inner edge of the bow head supporting the attached hair. Symmetry restricts motions to the x- and y-directions for the in-plane stick modes and to the z-direction alone for the out-of-plane modes. Note the lifting of degeneracy of the low frequency modes, resulting from the geometry of the bow stick, head and frog, and the irregular orderings of the higher in- and out-of-plane bending modes resulting from their coupling to the longitudinal and torsional vibrations, respectively. The measured and computed modes are the independent *normal* modes describing their coupled motions.

For relatively weakly damped normal modes ($Q \gg 1$), damping is only important in the immediate vicinity of a resonance, so that the x-direction admittance from all modes can be written as

$$A_x(f) = \sum_n \frac{if}{2\pi m_{n,x}[f_n^2(1 + i/Q_n) - f^2]} \tag{6}$$

with similar expressions for the admittance in the y- and z-directions.

TABLE II. Computed frequencies and effective masses at the point of hair attachment to the head of the bow of the in-plane (xy) and out-of-plane (zx) "bending" modes of a freely supported, Vuillaume-Tourte tapered bow stick and attached frog.

Frequency (Hz)	In-plane	Out-of-plane	m_z (g)	m_y (g)	m_x (g)
50.7	⋆			8.2	465
56.3		⋆	26.9		
141.1	⋆			12.3	181
143.2		⋆	8.30		
279.9	⋆			20.8	60.1
293.6		⋆	38.0		
467.7	⋆			37.9	47.1
468.9		⋆	11.4		
698.0	⋆			82.3	22.3
710.4		⋆	9.9		
901.3		⋆	2.1		
979.0	⋆			214	20.6
1106		⋆	3.4		
1288	⋆			$3.2\ 10^3$	10.6
1400		⋆	13.9		
1665	⋆			$2.8\ 10^3$	10.3
1771		⋆	62		
2030	⋆			164	5.9
2167		⋆	27.5		
2328		⋆	3.4		
2524	⋆			85.6	6.4
2711	⋆			112	12.3
2754		⋆	8.0		
3179	⋆			144	19.6
3273		⋆	14.7		
3561	⋆			41	6.9
3873		⋆	16.9		
4180		⋆	11.6		
4221	⋆			38	8.5
4543		⋆	7.7		

Figures 4(a) and 4(b) show plots of the real part of the computed frequency dependencies of the in-line admittances at the edge of the head of the bow using the effective masses computed above with "typical" Q_n-values of 30 for the freely supported bow. If measured Q-values were available, the height of each resonance would simply be scaled by the measured value.

The admittances have been plotted on a logarithmic scale to accommodate the large changes in magnitude with frequency. Frequencies have been plotted on a square root scale, which would give regularly spaced resonances for bending waves on a simple slender beam.

Consider first the two lower traces in Fig. 4 describing the in-plane admittances. At low frequencies, the admittance peaks in the transverse y-direction bending modes of the stick are initially considerably larger than those in the longitudinal x-direction. However, as the frequency increases, the increasingly large hatchet-like rotations of the head of the bow lead to larger deflections along the length of the bow than in the transverse direction, as can be seen from the mode shapes in Fig. 2. As a result, above around 400 Hz, the bending wave displacements of the inner edge of the bow head supporting the stretched hairs are dominated by motion along rather than displacement perpendicular to the length of the bow.

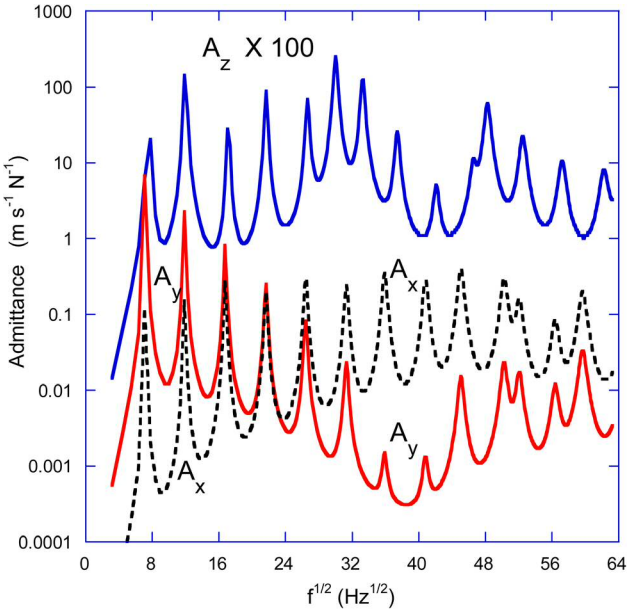

FIG. 4. (Color online) The real part of the computed admittances of the untensioned bow stick at the hair-supporting edge of the bow head, for in-line forces in the x, y, and z directions. The frequency is plotted on a $f^{1/2}$ scale. The lower two admittances A_x and A_y show the resonances of the in-plane vibrational modes with displacements parallel and perpendicular to the length of the stick. The upper curve A_z shows the out-of-plane mobility from transverse stick vibrations perpendicular to the length of the bow. A_z has been multiplied by 100 to distinguish it from the in-plane admittances. The Q-values of all resonances have arbitrarily been set to 30.

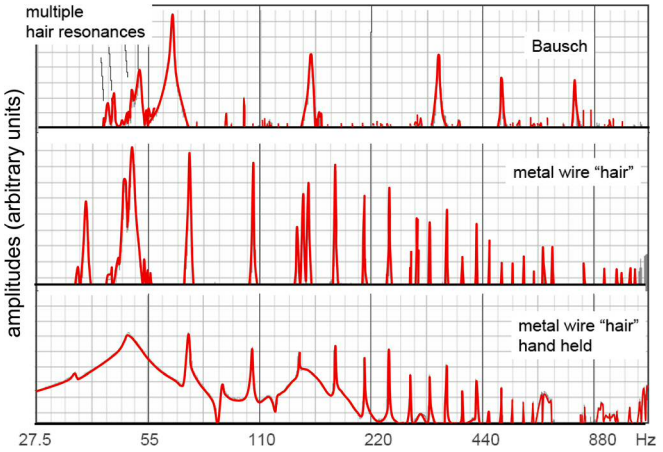

FIG. 5. (Color online) Time-delayed FFT spectra for the in-plane transverse vibrations of a fine bow by Bausch and an experimental bow with a wire of similar mass (~4 g) replacing the stretched hair. The upper two spectra are for the freely supported bows, while the bottom spectrum is for the experimental bow held firmly by the player in the normal way.

In addition, the need to conserve linear momentum involving the hatchet-like rotations of the bow head results in a strong coupling between the bending and longitudinal vibrations of the bow. This gives rise to an additional peak in the admittance at around 2700 Hz from the coupled $\lambda/2$ longitudinal resonance of the bow.

The upper trace shows the computed admittance for the out-of-plane transverse bending modes multiplied by 100 to differentiate it from the in-plane admittances. In this case, the varying heights and irregular spacings of the resonances result from the strong coupling between the transverse bending and torsional vibrations of the stick induced by the sideways swinging rotations of the head and frog of the bow.

D. Coupling to tensioned bow hairs

1. Experimental

If the bow stick modes are to influence the sound via the radiative modes of the body of the instrument or by influencing the slip-stick excitation of Helmholtz kinks, they can only do so via their coupling to the tensioned bow hairs in contact with the string.

Figure 5 compares fast Fourier transform (FFT) spectra obtained from impulse response measurements on a fine bow by Bausch and an experimental bow, with the horse hair replaced by a tensioned guitar string of similar mass (~4 g) and bow tension. Such a replacement circumvents the problem of the variations in lengths and physical properties of the individual hairs making up the ribbon of bow hair, which results in highly non-linear stretching properties at low tensions.[4] Impulse responses were measured with a miniature accelerometer (0.4 g) mounted on the head of the bow.

The upper two spectra compare the resonances of the freely supported Bausch bow and experimental bow. The bottom spectra illustrates the dramatic increase in damping of the stick resonances, when the bow is held by a player in the normal way.

The spectra for the lightly tensioned Bausch bow, reveals at least four, heavily damped, low frequency "hair" resonances below the lowest stick resonance at ~65 Hz, but little evidence for additional hair modes at higher frequencies. This can be explained by the variation of hair properties across the width of the ribbon resulting in a number of separate sections of the ribbon tending to vibrate independently of each other with slightly different resonant frequencies. Mutual friction within and between such sections would account for the large damping observed, in addition to locking the vibrations of adjacent sections together. In practice, the hair tension has to be increased to a significant fraction of the normal playing tension of around 60 N before any higher modes of hair vibration become clearly defined.

In contrast, many weakly damped higher-order modes are observed when the bow hair is replaced by the flexible guitar string of similar mass. This demonstrates that, in practice, the damping of hair vibrations is largely due to the variation in mechanical properties of the individual hairs rather than their coupling to the stick vibrations.

For both the Bausch and experimental bow, a number of well-defined, weakly damped, stick resonances can be identified. However, on holding the bow in the normal way, the damping of such modes increases dramatically, as illustrated by the lowest set of measurements. This suggests that the intrinsic damping of the wood used for making the bow stick is unlikely to be important in any assessment of the playing qualities of a bow.

Figure 6 illustrates the affect of the bow-hair interaction on the resonant frequencies of the lowest two normal modes of the experimental bow with the tensioned guitar string replacing the normal hair. The variations in normal mode

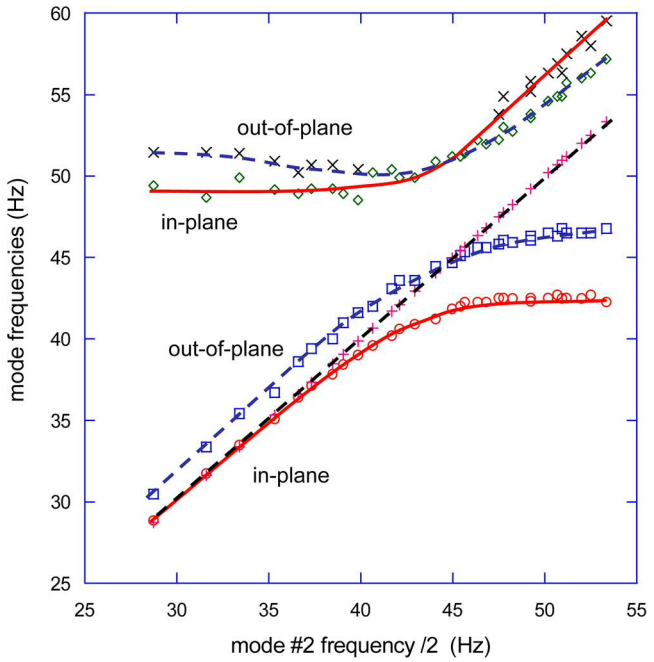

FIG. 6. (Color online) The normal mode frequencies of an experimental violin bow with the hair replaced by a metal wire of similar mass measured as a function of increasing "hair" tension. The modal frequencies are plotted as a function of increasing tension represented by half the measured frequency of the second hair mode, which is less strongly perturbed by the coupling to the stretched bow "hair." The smooth lines drawn through the experimental points are simply guides for the eye to distinguish the in-plane from the out-of-plane normal modes. The dashed line is half the frequency of the second "hair" mode, which indicates the overall slope expected for the hair resonance, in the absence of coupling to the stick vibrations.

frequencies are plotted as a function of increasing tension represented by half the measured frequency of the second "hair" resonance at $\sim\sqrt{T/m\ell}$, as this mode is much less strongly perturbed from coupling to the bow stick than the fundamental.

By tapping the bow in different directions and positions along the bow stick, with the measurement axis of the accelerometer changed accordingly, it was possible to identify the frequencies of the coupled mode vibrations in both the in- and out-of-plane directions, as indicated by the lines drawn through the measurements as guides to the eye.

The measurements illustrate the strong coupling between the stick vibrations and transverse hair vibrations. This leads to the familiar veering and splitting of the normal mode frequencies as the resonant frequencies of the coupled vibrations approach and cross each other.

As the tension increases, the frequency of the lowest normal mode deviates markedly below that of the uncoupled "hair" resonance, with the normal mode acquiring an increasing component of the lowest frequency stick vibrations. When their uncoupled frequencies would otherwise cross, the normal modes are split in frequency by an amount proportional to the strength of the coupling, which is slightly larger for the in-plane than the out-of-plane vibrations. At coincidence, the two normal modes involve the stick and stretched bow hair vibrating together in- and out-of-phase, with equal energy and damping. This results in split resonances of almost equal strength and widths.

At higher tensions the component of hair vibration in the lowest normal modes decreases, with the lowest mode transforming smoothly into that of a slightly depressed frequency stick mode. Similarly, as the tension increases from zero, the initial stick mode transforms smoothly into a mode dominated by the hair vibrations.

At low tension, the frequency of the out-of-plane stick vibrations is slightly larger than the in-plane frequency. Furthermore, the measurements suggest a slight decrease in resonant frequency with increasing tension along the length of the stick. This is consistent with the predicted decrease in resonant frequency of a straight stick, when the tension becomes a significant fraction of the critical Euler buckling tension of ~70 N.[13] In contrast, the frequency of the in-plane "stick" mode initially remains almost constant as the camber is decreased on increasing tension.

The strong coupling between the lowest vibrational modes of the bow and the stretched bow hair may well contribute to the "feel" of the hand-held bow. Such coupling will result in the transfer of an appreciable amount of low frequency energy to the bow from the tensioned hair in contact with the vibrating string. This energy could, in principle, be sensed by the player holding the bow, even though the stick vibrations themselves radiate very little sound. The strength of such coupling will depend on the height of the bow tip, the bow tension, the bending and taper of the bow and the relative masses of bow and stretched bow hair.

In practice, both the in-plane and out-of plane modes of the bow may contribute to the players "feel" of a bow, as the bow is usually inclined at an angle away from the bridge, so that both in-plane and out-of-plane bending modes will be excited.

E. Influence of bow on radiated sound

In a preliminary investigation of the potential influence of bow vibrations on the sound of the violin, the sound pressure was measured at the "acoustic center" of the violin cavity (on the central axis approximately in line with the *f*-hole notches). Measurements were made before and after resting a bow halfway along the bow hair on the inner two strings close to the bridge, which was give a short tap in the bowing direction on its upper bass-side corner, as plotted in Fig. 7.

With such a microphone placing, at an antinode of finite-element computed *A1* (500 Hz) and *A2* (1154 Hz) internal air resonances, the internal sound pressure below ~1 kHz is almost entirely determined by the coupling of the violin plate vibrations to the low frequency Helmholtz air vibrations at ~290 Hz and the significantly higher frequency *A3* (1212 Hz) mode. The resonantly excited internal sound pressure is then closely related to the radiated monopole sound intensity radiated by the signature *A0, CBR, B1-*, and *B1+* signature modes. At higher frequencies, the internal sound pressures will still be proportional to the intensities of the increasingly directional radiated sound. Any changes in the internal sound pressures will therefore reflect similar changes in the radiated sound pressures.

Comparison of the two sets of measurements shows that placing the bow on the violin makes very little difference in

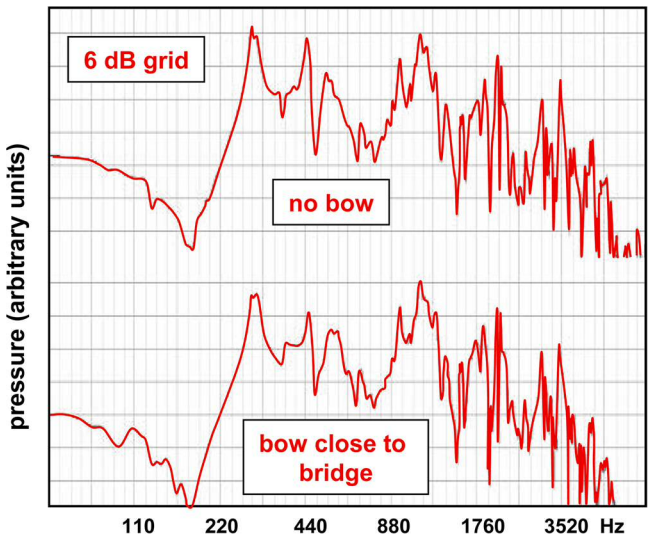

FIG. 7. (Color online) Sound pressure at the acoustic center of the violin cavity of a Vuillaume violin with damped strings tapped at the bass-side corner of the bridge in the bowing direction (upper curve) and repeated (lower curve) with a violin bow pressed firmly down on the middle two strings close to the bridge halfway along the bow hair. The two sets of measurements have been shifted relative to each other for easy comparison.

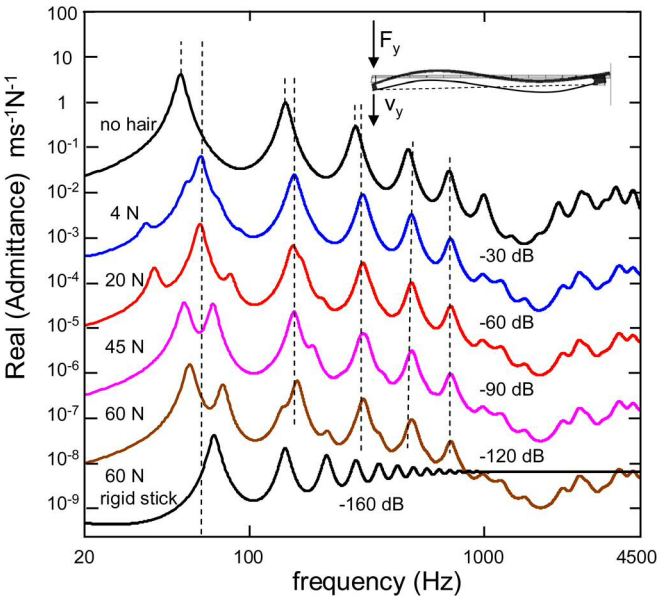

FIG. 8. (Color online) The frequency dependence of the real part of the admittance at the head of the bow for a sinusoidal force in the direction shown. The uppermost curve is for the freely supported bow without attached bow hair and the lowest plot for the admittance of the bow hair alone at a tension of 60 N. The plots between are for the bow with attached bow hair, at tensions 4, 20, 45, and 60 N, with each succeeding plot shifted relative to each other by −30 dB for clarity. The lowest plot is the input admittance for transverse waves on the bow hair at tension 60 N on the same scale but reduced in value by 160 dB.

the recorded sound, especially above 1 kHz, apart from a slightly reduced response above around 3 kHz. This is almost certainly due to the additional mass loading of the bow resting on the bridge.

Below the strong *A0* resonance at around 290 Hz, the bow introduces some additional weak structure, which may well result from low frequency stick and hair resonances. However, even in this strongest possible coupling case, the changes in sound levels are typically only around 1 dB or less and are unlikely to be perceptually significant. The measurements also suggest the bow slightly increases the damping of the signature *A0* and *B1*- modes and contributes some additional weak structure in the range 300–500 Hz, which may also be related to bow resonances.

Such features are small and would be significantly smaller if the bow had been placed at a normal bowing position along the strings. Nevertheless, it would be interesting to pursue such measurements further, to place more reliable upper limits on the possible contribution of the bow's induced vibrations to the radiated sound. Independent measurements of the radiated sound produced by the tapped violin stick alone show that any direct radiation from the stick is extremely small—almost certainly much less than the 30 dB difference in radiated sound pressure observed for similar strength taps on the violin bridge and directly on the bow stick when raised slightly off the string.

F. Theoretical model

The coupling of the freely supported bow stick vibrations to the transverse and longitudinal vibrations of the hair can be represented by loading the head end of the stick by the input impedances Z_T and Z_L of equivalent open-ended transmission lines—ignoring the smaller stick vibrations at the frog.

The loading of the hair is assumed to leave the vibrational mode shapes of the stick unchanged, though the coupling will affect the frequencies and strengths of the resulting new set of normal modes describing the coupled vibrations of the stick and both longitudinal and transverse hair vibrations.

First consider the response of the coupled system to an in-plane sinusoidal force $F_y e^{i\omega t}$ at the head of the bow in a direction perpendicular to the stretched bow hair, as illustrated by the inset in Fig. 8. Each in-plane bow stick mode involves velocities at the hair-supporting head end of the stick at a mode-dependent angle θ_n to the applied force. This angle can be related to the effective masses for local velocities along the transverse (T or y), longitudinal (L or x), or θ_n directions. The kinetic energy of a mode can be expressed in terms of the local velocities, such that $\frac{1}{2}m_{n,T}v_{n,L}^2 = \frac{1}{2}m_{n,L}v_{n,L}^2 = \frac{1}{2}m_n v_n^2$, so that $\tan^2\theta_n = m_{n,T}/m_{n,L}$. Table I lists the effective masses of the first 14 freely supported dynamic stick modes below 4.6 kHz for the finite element modeled Tourte-tapered bow.

Initially, damping will be ignored. The dynamics of each stick mode is then equivalent to that of a mass m_n forced to slide on an inclined plane at a mode-dependent angle θ_n. Its motion is subject to its own in-line restoring force determining the modal frequency ω_n in addition to the θ_n-components of any applied forces—in this example, forces from transverse and longitudinal waves excited on the bow hair. Such forces are determined by the sum of induced velocities from all excited stick modes, $V_L = \sum v_{n,L} = \sum v_n \sin\theta_n$ and $V_T = \sum v_{n,T} = \sum v_n \cos\theta_n$, flowing into the input impedances Z_L and Z_T of the acoustic transmission lines.

For a given mode, the velocity v_n along the constraining angle θ_n is then given by

$$m_n[i\omega + \omega_n^2/i\omega]v_n = (F - Z_T V_T)\cos\theta_n - Z_L V_L \sin\theta_n. \tag{7}$$

V_T and V_L can be determined self-consistently by summing the component velocities from all the stick modes, so that

$$V_T = \left[\sum \frac{i\omega}{m_{n,T}[\omega_n^2 - \omega^2]}\right](F - Z_T V_T) - \left[\sum \frac{i\omega}{\sqrt{m_{n,T}m_{n,L}}[\omega_n^2 - \omega^2]}\right] Z_L V_L, \tag{8}$$

$$V_L = \left[\sum \frac{i\omega}{\sqrt{m_{n,T}m_{n,L}}[\omega_n^2 - \omega^2]}\right](F - Z_T V_T) - \left[\sum \frac{i\omega}{m_{n,L}[\omega_n^2 - \omega^2]}\right] Z_L V_L, \tag{9}$$

with the trigonometric functions described in terms of effective masses.

The admittance in the driving force direction, $A_T = V_T/F_T$, is then given by

$$A_T = \frac{A_{TT} + (A_{LL}A_{TT} - A_{TL}^2)Z_L}{(1 + A_{TT}Z_T)(1 + A_{LL}Z_L) - A_{LT}^2 Z_T Z_L}, \tag{10}$$

where the admittances A_{TT}, A_{LL}, and A_{TL} are given by the summations in square brackets in Eqs (8) and (9).

Damping can be incorporated by adding a dissipative term to the modal frequencies of the freely supported stick, with $\omega_n^2 \to \omega_n^2(1 + i/Q_n)$, and complex propagation constants for the lossy transmission lines, such that $Z_T = \sqrt{Tm/\ell}/\tanh(\zeta_T \ell)$ with $\zeta_T = \omega(1 - i/Q_T)/c_T$ and $Z_L = \sqrt{E\rho S}/\tanh(\zeta_L \ell)$ with $\zeta_L = \omega(1 - i/Q_L)/c_L$, where $c_T = \sqrt{T\ell/m}$ and $c_L = \sqrt{E/\rho}$ are the speeds of transverse and longitudinal waves along the ribbon of hair of mass m and cross-sectional area S stretched to a tension T (see, for example, Ramo *et al.*,[17] Table 1.23).

In the absence of coupling to the longitudinal modes of hair vibration ($Z_L = 0$), Eq. (10) reduces to

$$A_T = \frac{1}{1/A_{TT} + Z_T}. \tag{11}$$

This has a simple interpretation, with the velocity in the driving force direction determined by the parallel combination of stick mode impedances in series with the input impedance of the transmission line modeling the transverse modes of vibration of the stretched bow hair.

Coupling to the longitudinal modes adds an additional channel for energy flow, leading to the rather more complicated expression in Eq. (10).

Figure 8 illustrates the predicted frequency dependencies of the real (in-phase) component of the admittance in-line with the driving force. The plots have been evaluated from the above equations using the computed effective masses listed in Table I. The ribbon of bow hair is assumed uniform along its length $\ell = 65$ cm, with 175 active hairs of elastic constant 5.5 GPa, density 1300 kgm^{-3} and diameter 0.2 mm giving a total mass of ~4.6 g—averages of values cited by Askenfelt.[4] For illustrative purposes, Q-values of 20 and 10 have been assumed for transverse and longitudinal waves on the bow hair and 10 for the stick modes. In practice, both the stick and hair vibrations are likely to be more heavily damped—especially when the bow is held by the player and at low bow tensions when individual hairs are tensioned by different amounts.

The upper two plots illustrate the slight increase in frequency of the "stick" frequencies on attaching the tensioned bow hair, which acts as a compressible spring at frequencies below its first longitudinal resonance at around 1.5 kHz. On increasing tension, stronger peaks from the transverse wave resonances become more evident. As the lowest transverse wave resonance approaches the lowest stick resonance at around 60 Hz, the familiar veering and splitting of the resulting normal mode resonances is observed, with a splitting comparable with measured values plotted in Fig. 6. The transverse wave hair resonances die out quite rapidly because of damping. At high frequencies the terminating impedance at the head of the bow from transverse waves is then simply the characteristic mechanical impedance $\sqrt{Tm_h/\ell}$, as illustrated in the lowest plot showing the real part of the input admittance of the equivalent transmission line.

On increasing bow tension, the lowest transverse hair resonance increases toward and eventually crosses the lowest "stick" resonance. This results in an appreciable veering and splitting of the resulting normal mode frequencies, as illustrated for tensions of 20, 40, and 60 N shifted relative to each other by 30 dB. The lower plot shows the input impedance of the transmission line with peaks at the resonant frequencies, with an impedance approaching the characteristic transmission line impedance $\sqrt{Tm/\ell}$ as the transverse wave resonances die out.

Such characteristics clearly describe important features observed in modal measurements on the bow stick. Of more direct musical importance is the potential influence of the stick modes on the excitation of sound via their influence on bow hair vibrations.

In an attempt to assess the importance of such coupling, the input admittance of the bow hair at its midpoint has been derived for excitation transverse parallel to and along the length the hair, as illustrated schematically by the inset in Fig. 9.

For example, the transverse impedance Z_{HT} is given by

$$Z_{HT} = \sqrt{Tm/\ell}\left[\frac{1}{\tanh(\zeta_T \ell/2)} + \frac{Z_{Tload}\cosh(\zeta_T \ell/2) + \sqrt{Tm/\ell}\sinh(\zeta_T \ell/2)}{\sqrt{Tm/\ell}\cosh(\zeta_T \ell/2) + Z_{Tload}\sinh(\zeta_T \ell/2)}\right], \tag{12}$$

where Z_{Tload} is the terminating impedance at the head end of the stretched bow hair presented by the stick modes and longitudinal waves on the stretched bow hair.

To evaluate Z_{Tload}, consider the response of each individual mode to a transverse driving force F at the head of the bow. This can be simply derived from Eq. (12) by setting $Z_T = 0$, so that

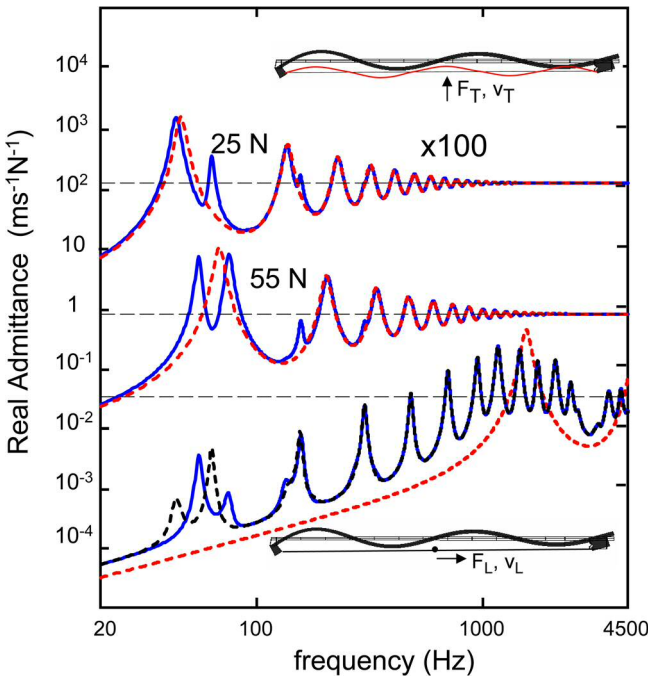

FIG. 9. (Color online) The frequency dependence of the real part of the admittance for transverse and longitudinal hair waves at the midpoint of a bow. The upper two plots are for transverse waves for bow tensions of 25 and 55 N (solid curves); the admittance for rigid end supports is shown by the dashed line. The lower plot is for longitudinal wave excitation at the same two bow tensions. The dashed curve is the midpoint admittance for the hair with rigid end supports. The dashed horizontal lines are half the corresponding characteristic transmission line admittances.

$$Z_{Tload} = \frac{1 + A_{LL}Z_L}{(A_{LL}A_{TT} - A_{TL}^2)Z_L + A_{TT}}. \tag{13}$$

Similarly, for longitudinal waves

$$Z_{Lload} = \frac{1 + A_{TT}Z_T}{(A_{LL}A_{TT} - A_{TL}^2)Z_T + A_{LL}}. \tag{14}$$

Figure 9 plots the real part of the midpoint bow hair admittance for both transverse and longitudinal waves, with Q-values for the stick, transverse, and longitudinal hair resonances of 30, 20, and 20, respectively, which allows direct comparison with admittance measurements by Askenfelt.[4]

The upper two plots show the transverse wave admittances for two bow tensions (25 and 55 N) with the lower tension plot increased by a factor of 100 for clarity. In both cases the admittance curve for rigid end supports is shown for comparison.

Because the hair is excited at its midpoint, only n-odd modes are excited. Apart from the anticipated veering and splitting of the lowest hair resonance by coupling to the fundamental stick resonance, the admittance is dominated by the transverse wave resonances of the bow hair. This suggests that coupling to the stick vibrations via the transverse bow-hair vibrations is most unlikely to contribute to the sound of the instrument other than possible influence of the lowest frequency transverse on the slip-stick mechanism.

The lowest solid curve shows similar data for the midpoint longitudinal excitation of the bow hair. The admittance is again plotted for two bow tensions—25 N (dashed curve) and 55 N (solid). The lowest dashed curve shows the longitudinal admittance for rigid end supports, with the first half-wave longitudinal stretched hair resonance at around 1.5 kHz. Apart from the influence of the transverse hair modes on the lowest stick mode, the response is dominated by the longitudinal stick resonances superimposed on a broadened resonant response from the longitudinal modes of the hair. The strong stick resonances are induced by the hatchet-like rotations of the head of the bow, which relaxes the rigid end constraint, particular at resonant stick frequencies. The admittance will also include a reactive inertial term $1/iM\omega \sim 3/if$, associated with rigid body motion. Although small, this will tend to mask the resonances below 1 kHz—as observed in the measurements by Askenfelt[4], which are otherwise in good quantitative agreement with the above predictions, though the heights of specific resonances clearly depend on assumed Q-values.

The above model assumes uniform hair ribbon properties, with longitudinal forces applied to the first layer of stretched bow hairs shared equally across the total thickness of the ribbon. In practice, this may not be justified. Nevertheless, if the coupled stick modes are to have any direct influence on the sound of the violin, the above model strongly suggests that coupling of the stick modes to the longitudinal modes of the bow hair are likely to be more important than coupling to the transverse modes.

III. BOUNCING BOW MODES

The above discussion has focused on the modes of the freely supported bow, whereas the modes of most importance for the player are those of the hand-held bow. While bowing, the bow is also subject to the additional constraint introduced by the bow hair pressing down on the string. Such constraints introduce a new set of low-frequency bouncing modes, which have a major influence on the downward force between bow hair and string at the start of any bowed note.

There are two types of bouncing modes—those in which the downward bow pressure maintains the bow contact with the string and another in which the bow is allowed to bounce on and off the string. An excellent overview of the importance of such modes when playing short repeated bowed notes is given by Guettler in a contributed chapter in *The Science of String Instruments*.[10]

A. On-string bouncing modes

Askenfelt[3] identified and published the first measurements of the *on-string* bouncing modes in the range 7–30 Hz depending on hair tension, stick moment of inertia I, and string contact position x from the frog-end of the bow hair. Bissinger[5] also investigated such modes in addition to *off-the-string* bouncing modes, which increased in repetition rates from 5 to 11 Hz over a few second interval, as the bounce energy was dissipated. Subsequently, Askenfelt and Guettler[7] developed a rigid stick, quasi-static, model for the on-string bounce frequency given by

$$f = \frac{1}{2\pi}\sqrt{\frac{Tx\ell}{I(\ell - x)}}. \quad (15)$$

In this section, finite element computations are described which illustrate how such modes are influenced by the lowest frequency stick vibrations. The Tourte-tapered bow is assumed to be pivoted about the frog end of the tensioned bow hair, with a rigid support at the point of contact with the string and an in-plane restoring force $Txy/\ell(\ell - x)$ at the head end of the bow hair, where y is the displacement. This assumes that sections of bow hair on either side of the bowing point remain straight, which is a good approximation for bounce frequencies much smaller than the transverse resonances of the deflected length of bow hair.

Figure 10 shows the computed bounce frequencies of the first two modes of the bow as a function of bowing point distance x along the bow hair, for tensions of 40 N (dashed lines) and 60 N (solid lines). The changes in the bow stick's modal shapes are also illustrated as a function of bowing position, with open and closed vertical wedges indicating the positions of the pivot and string-supported point along the bow hair. The dotted line shows the bounce frequency predicted by the rigid stick model, Eq. (15) rising from zero at the frog-end to infinity at the head-end of the bow hair.

Over the lower half of the bow, the computed lowest bounce mode frequencies are virtually identical to those predicted by the quasi-static model. However, as the bowing point moves toward the upper end of the bow, the bounce frequency drops well below the rigid-stick predictions. A limiting frequency is reached corresponding to the lowest vibrational mode of the pivoted bow simply supported at the point of attachment to the bow hair. Conversely, as the contact point approaches the frog, the bounce frequency approaches zero, corresponding to the inertial rotation of the bow about the pivot point.

The higher-order pivoted stick modes are also strongly perturbed by placing the bow on the string, as illustrated for the second coupled stick and bow hair mode. With the bowing point close to the frog, the head end of the bow is essentially freely supported. This results in a bending wave antinode at the end of the stick and a node around a quarter of the way along its length. However, as the bowing point nears the end of the bow, the head displacement is increasingly constrained, forcing the node to move inward toward the middle of the stick, with two half-wavelengths along its length and a corresponding large increase in mode frequency.

In practice, the string at the point of contact is not ideally rigid, but will deflect slightly under the influence of the deflected tension in the bow hair. Askenfelt[2] estimated that this would reduce the bounce frequency on the G-string by typically ~15%.

Figure 11 shows measurements of the first two bouncing modes of a Bausch bow. The first two resonant frequencies of the deflected lengths of hair are also plotted. Because these frequencies are appreciably larger than the low frequency bouncing frequencies, the straight bow hair approximation is justified for the lowest bouncing mode. It is therefore unlikely that coupling to the dynamic hair modes would significantly influence the measured bounce rates, other than for the second stick mode, for a bow point close to the frog.

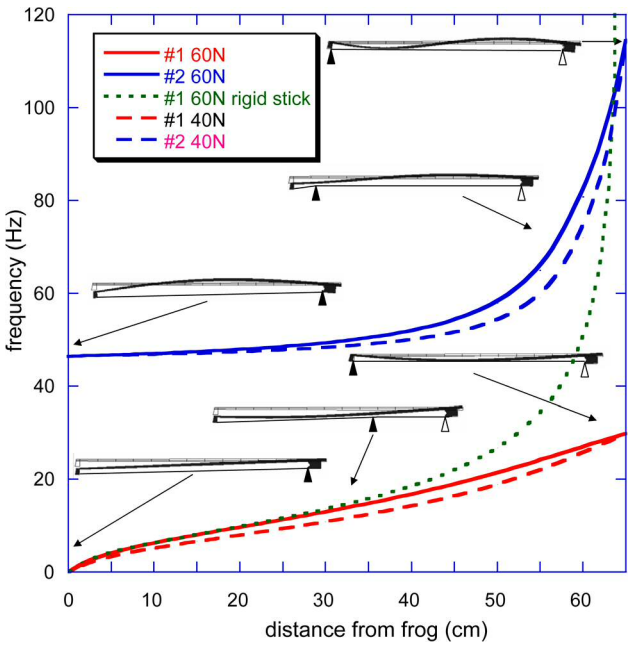

FIG. 10. (Color online) The frequency of the first two bouncing modes of a Tourte-tapered bow at bow tensions 60 N (solid) and 40 N (dashed), pivoted (open triangles) about the frog-end of the bow hair, with the hair in contact with the assumed rigid string (closed triangle), as a function of bowing position along the length. Representative modal shapes are also shown for string contact points at the ends of the bow and for intermediate positions. The dotted line shows the quasi-static, rigid bow stick predictions.

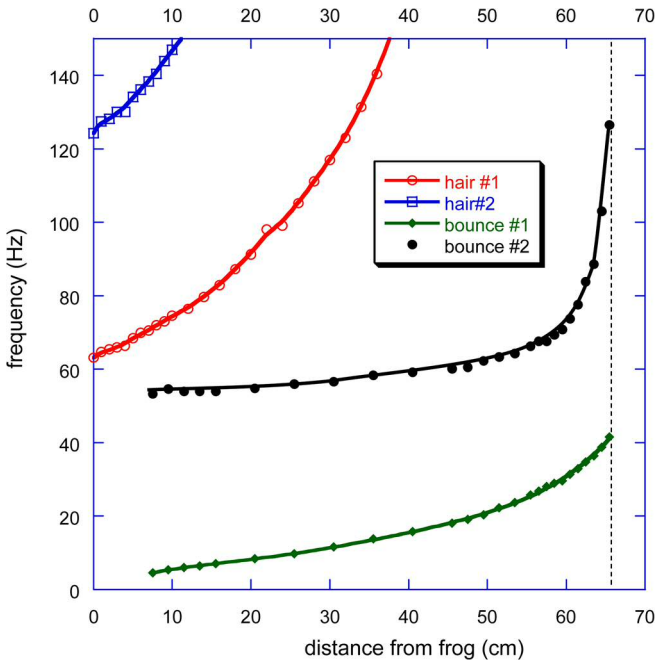

FIG. 11. (Color online) Measurements of the first two on-string bouncing mode frequencies, for a bow by Bausch pivoted about the frog, as a function of the distance of a rigid support from the frog end, for a typical playing tension of around 50–60 N.

B. Off the string modes

For large impact velocities, the bow will hit the string, undergo a half-period τ_{on} bouncing cycle on the string, then be thrown off, reversing the initial angular momentum at impact. Under the influence of a restoring couple C from gravity and the player's fingers, the bow will return to the string after a time τ_{off}, with a net bounce rate given by

$$f_{on-off} = 1[\tau_{on} + \tau_{off}] \tag{16}$$

$$= 1/\left[\pi\sqrt{I(l-x)/Tx} + 2I[d\theta_d/dt]_o/C\right]. \tag{17}$$

To obtain a regular sequence of repeated bounces, the player can compensate for the increase in bounce rate from damping, by decreasing the downward couple on the bow or by moving the point of contact further towards the upper end of the bow, or a combination of both.[10]

Eventually, the losses will result in bouncing modes of smaller amplitude than the static deflection of the bow hairs, $\theta_{static} = C_{static}(\ell - x)/T\ell x$.

The bow will then have insufficient energy and vibrational amplitude for the bow to bounce off the string. The hair will then remain on the string and execute decaying vibrations of small amplitude at the on-string bounce rate.

In the intermediate regime, when the amplitude of stick vibration is comparable with the static deflection, the bow will spend longer on the string than half a period and will leave the string with a velocity less than its maximum amplitude. As the bouncing amplitude decreases, the bow will progressively spend less time off the string until the amplitude reaches that of the static deflection, as observed by Bissinger.[5] The bow will then continue to vibrate at the on-string vibrational frequency.

In practice every bow has a "sweet point," where the player finds it easy to bounce the bow. This is usually slightly above the midpoint of the bow, close to, but slightly above, the center of percussion. This reduces the impact on the hand holding the bow, allowing the player to maintain sufficient control of the downward force to control the bounce at the start of every note. As the contact point moves toward the frog, the impact on the bowing hand increases and it becomes progressively harder to control the bow and make use of the natural bouncing modes. The bow then has to be bounced on and off the string by vertical motions of the hand holding the bow, with the fingers holding the bow having to control the low frequency bouncing modes excited every time the bow hits the string. Such low frequency vibrations result in relatively large oscillations of the downward pressure of the hair on the string, as demonstrated by Guettler.[9]

A player will identify the quality of a bow, at least in part, with the ease with which all such bouncing modes can be controlled. In the lower part of the bow, the quality will be almost entirely dependent on its inertial properties and the playing tension, while in the upper half the quality will be increasingly dominated by the frequency of the 30–40 Hz resonances of the pivoted stick resting on a rigid end support.

IV. SUMMARY

Finite element, analytical models and measurements on real and experimental bows have been used to investigate the dynamical properties of bows with and without attached bow hair. Computations on a Tourte-tapered bow stick with attached frog and bow head illustrate relatively strong coupling between the bending waves of the stick and its torsional and longitudinal vibrations. The computations identify both modal frequencies and effective masses at the hair-supporting end of the bow. These masses are used to obtain the admittance of the freely suspended bow and the admittance at the midpoint of the bow hairs, in both transverse and longitudinal directions.

Measurements with an experimental bow, with the bow hairs replaced by a flexible guitar string, demonstrate the strong coupling between the lowest stick modes and those of the stretched bow hairs. However, no significant change in the acoustically radiated sound was observed when the bow was pressed firmly down on the bridge. This suggests that any direct coupling of the bow vibrations, via the stretched bow hair and bridge to the radiating surfaces of the instrument is very small.

The bouncing modes of the pivoted bow resting on the string have also been computed and investigated experimentally. Such computations demonstrate how the bounce rate in the upper half of the bow is strongly influenced by the lowest frequency vibrational modes of the bow stick, refining an earlier quasi-static model for bounce rates derived by Guettler and Askenfelt.[7–9]

This investigation has revealed a rich menagerie of bow vibrations. However, there remains little evidence that any of the stick modes excited by bowing the string will interact sufficiently strongly with the vibrations of the body to make a significant contribution to the radiated sound, other than via their possible influence on the slip-stick excitation of Helmholtz kinks circulating around the bowed string.

ACKNOWLEDGMENTS

The comments from referees on an earlier draft of this paper are gratefully acknowledged, in addition to the advice and feedback from several colleagues attending Oberlin Violin Acoustics Workshops including John Aniano, John Graebner, Norman Pickering, Joseph Regh, and Fan Tao.

[1]R. Schumacher, "Some aspects of the bow," Catgut Acoust. Soc. Newsl. **24**, 5–8 (1975).
[2]A. Askenfelt, "Observations on the dynamic properties of violin bows," STL-QPSR **33**(4), 43–49 (1992), http://www.speech.kth.se/qpsr (Last viewed 2/15/2012).
[3]A. Askenfelt, "A look at violin bows," STL-QPSR **34**(2-3), 41–48 (1993), http://www.speech.kth.se/qpsr (Last viewed 2/15/2012).
[4]A. Askenfelt, "Observations on the violin bow and the interaction with the string," STL-QPSR **36**(2-3), 107–118 (1995), http://www.speech.kth.se/qpsr, (Last viewed 2/15/2012).
[5]G. Bissinger, "Bounce tests, modal analysis, and playing qualities of violin bow," J. Catgut Acoust. Soc. **2**, 17–22 (1995).
[6]G. Bissinger and K. Ye, "Effect of holding on the normal modes of an instrumented violin bow," Proc. SPIE **3727**, 126–130 (1999).
[7]A. Askenfelt and K. Guettler, "The bouncing bow: Some important parameters," TMH-QPSR **38**(2-3), 53–57 (1997), http://www.speech.kth.se/qpsr (Last viewed 2/15/2012).

[8]A. Askenfelt and K. Guettler, "Quality aspects of violin bows," J. Acoust. Soc. Am. **105**, 1216 (1999).
[9]A. Askenfelt and K. Guettler, "On the kinematics of spiccato and ricochet bowing," J. Catgut Acoust. Soc. **3**(6), 9–15 (1997).
[10]K. Guettler, "Bows, strings, and bowing," in *Science of String Instruments*, edited by T. D. Rossing (Springer, New York, 2010), Chap. 16, pp. 279–299.
[11]J. Woodhouse and P. M. Galluzzo, "The bowed string as we know it today," Acta. Acust. Acust. **90**(4), 579–589 (2004).
[12]L. Cremer, *The Physics of the Violin*, translated by John S. Allen (MIT Press, Cambridge, 1983), Sec. 5.2, pp. 79–83.
[13]C. Gough, "The violin bow: Taper, camber and flexibility," J. Acoust. Soc. Am. **130**, 4105–4116 (2011).
[14]N. Fletcher and T. D. Rossing, *The Physics of Musical Instruments: Second edition* (Springer, New York, 1998), Sec. 2.6, pp. 60–63.
[15]Comsol Multiphysics 3.2: Structural Mechanics Module (Comsol Ltd, London, 2005).
[16]F. Fétis, "D'analyses théoretiques sur l'archet (A theoretical analysis of the bow)," in *Antoine Stradivari-Luthiere célèbre des Instruments a archet* (*Notice of Anthony Stadivari: The Celebrated Violin Maker*) (Vuillaume, Paris, 1856), translated by J. Bishop (1864), http://www.archive.org/details/noticeofanthonys00feti (Last viewed 2/15/2012).
[17]S. Ramo, J. R. Whinnery, and T. van Duzer, *Fields and Waves in Communication Electronics* (Wiley, New York, 1965), Table I.23, p. 46.